Journal of Non-Crystalline Solids 575 (2022) 121199

Contents lists available at ScienceDirect

Journal of Non-Crystalline Solids

journal homepage: www.elsevier.com/locate/jnoncrysol

Luminescence of ODC(II) in quartz and cristobalite glasses

Tatiana Garmysheva [a], Alexander I. Nepomnyashchikh [a], Alexey Shalaev [a], Ekaterina Kaneva [a], Alexey Paklin [a], Kirill Chernenko [b], Anna P. Kozlova [c], Vladimir Pankratov [d], Roman Shendrik [*,a]

[a] Vinogradov Institute of geochemistry SB RAS, 1a Favorskogo str., Irkutsk, 664033, Russia
[b] MAX IV Laboratory, Lund University, Lund, SE-22100, Sweden
[c] NUST MISIS, 4 Leninsky prospekt, Moscow,119049, Russia
[d] Institute of Solid State Physics, University of Latvia, 8 Kengaraga Iela, Riga LV-1063, Latvia

ARTICLE INFO

Keywords:
Silica glass
Ge-ODC
Luminescence
VUV excitation
GLPC

ABSTRACT

The results of the optical spectroscopy of twofold coordinated silicon centers – ODC(II) in quartz and cristobalite glasses are presented. The luminescence and excitation spectra attributed to different local symmetry of ODC(II) were investigated under synchrotron excitation in the VUV region. The observed differences in the luminescence and excitation spectra of ODC(II) are caused by the environment and, therefore, short-range order in the samples.

1. Introduction

The study of localized electronic excitations in disordered materials is essential for understanding of the mechanisms of the formation of short-range within the basic unit of SiO_4 tetrahedra and intermediate-range orders. Some basic properties of the excitations, such as the structure of their excited states, are mainly determined by short-range order. Therefore, optical spectroscopy techniques are the sensitive method to determine the changes in the short-range order in glasses [1–4].

One of the widespread local defects in silica glasses is the twofold coordinated silicon centers – ODC(II), which are detected by the absorption band at 5.0 eV [5]. These defects can be observed in irradiated glasses [3], and affected by a heat treatment in reduced atmosphere or silicon vapor [6–8]. The samples containing ODC(II) exhibit the characteristic luminescence bands at 3.2 and 4.3 eV which are associated with triplet-singlet and singlet-singlet transitions in ODC(II), respectively [3]. In the case of silica doped with germanium, the luminescence of Ge-ODC(II) or GLPC can also be observed in the same spectral region, and these glasses are widely studied elsewhere [9]. It has also been shown that the spectral position of the luminescence bands as well as their halfwidth are strongly dependent on a local environment of the ODC(II) [8,10–13].

At room temperature, the triplet-singlet band peaking at 3.2 eV is usually more intense than the singlet-singlet band at 4.3 eV. However, the intensity of the triplet-singlet band can be decreased as a result of chemical or radiation treatment of glasses [2,14,15].

In several studies was found that a glass can inherit intermediate-range orders during its formation [16]. The positions of the luminescence, absorption, and excitation bands of ODC(II) behave similarly in glasses and in single crystals with similar structure [1,17]. On the other hand, the peak position of absorption bands, especially the high-energy bands are often determined by the local environment of the ODC(II) [8,11,18,19]. Thus, the optical properties of these centers can be used as a probe that shows the change in the short-range order in the glass depending on, for example, the phase composition of the raw materials.

In this work, we studied the luminescence properties of ODC(II) centers in quartz and cristobalite glasses. Cristobalite glass is more resistant to crystallization than quartz glass [20]. Earlier in [21] it was shown that E' centers have a different structure in irradiated cristobalite in comparison with quartz glasses. This fact could be explained by the difference in short-range order in the samples. In this study, the luminescence characteristics of cristobalite and quartz glasses are investigated under vacuum ultraviolet (VUV) excitations to reveal the difference in short and medium range order in these two modifications of glasses.

* Corresponding author.:.
E-mail address: r.shendrik@gmail.com (R. Shendrik).

https://doi.org/10.1016/j.jnoncrysol.2021.121199
Received 17 August 2021; Received in revised form 24 September 2021; Accepted 26 September 2021
Available online 1 October 2021
0022-3093/© 2021 Elsevier B.V. All rights reserved.

2. Methodology

2.1. Synthesis

Polycrystalline natural quartz from Bural Sardyk deposit was used as a raw material. Bural-Sardyk is located in the East Sayan Mountains and contains very pure polycrystalline quartz [22,23]. The raw material consists of grains of alpha quartz having an average size of 100 μm. The impurities of hydroxyl groups and water have not been found in the raw material [24]. It was chemically enriched and contains no more than 10 ppm of metal impurities according to ICP-MS analysis [20]. The concentration of Al is less than 1 ppm according to electron paramagnetic resonance (ESR) analysis. The concentration of Ge impurity is about 1.4 ppm [23] obtained by ICP-MS. According to powder XRD, the sample contains only α-quartz. This raw was used to make a silica glass, denoted as the sample A.

Another glass sample was prepared from the raw material, which was exposed at a temperature of 1450 °C for 48 hours and cooled down to room temperature. According to the powder XRD, the content of β-cristobalite increases significantly up to 80%, while the content of α-quartz decreases to 20% of the entire phase composition in the raw material.

It was used to produce glass, which we refer as the sample B. Varying the heating time in the range 24–48 hours at temperature 1450 °C led to the change of relationship between phases of β-cristobalite and α-quartz in the raw material.

The melting of the raw material was produced in graphite crucible using graphite heater element in the reducing atmosphere to create a large amount of ODC(II) in silica glasses.

2.2. X-ray diffraction

X-ray diffraction (XRD) patterns were obtained at room temperature on a Bruker D8 ADVANCE powder diffractometer (Cu $-$ $K_{\alpha1,\alpha2}$) radiation, 40 kV, 40 mA) with a linear VANTEC detector. The patterns were obtained between 2θ 5° and 70° with the step size 0.02°, and the counting time at about one second per step. Powder samples for measurements were prepared by packing and leveling in a special cuvette. All peaks of the powder X-ray diffraction pattern were indexed and several phases were identified, i.e. quartz and cristobalite (Figure 1S in the Supplementary materials). The structural models of these phases from the TOPAS structural database (Release 2006) available in the PC software package DIFFRAC-PLUS supplied from Bruker were taken as a starting for the multiphase Rietveld refinement method [25]. A quantitative analysis was performed by means of TOPAS 4.2 [26] software package. Refinements were stable and gave relatively low R-factors (5.0–6.1%). The TOPAS 4.2 was also used to determine the crystallinity index of samples. The amorphous component of the diffraction patterns was considered as the glass phase. The halo of the reflection corresponding to diffuse scattering was described independently in the form of some bell-shaped function. The Pseudo-Voigt line shapes were used for both crystalline and amorphous phases. A three-parameter of 2nd order polynomial function was utilized for the background curve. The degree of crystallinity was calculated from the area of the crystalline phase divided by the total area of crystalline and amorphous phases. The measured patterns were refined without any corrections or other processing; Lorentz-polarization, absorption, and sample displacement corrections were applied to the calculated patterns.

2.3. Spectroscopy

The samples have been cut in 2 mm thickness plates and polished for optical experiments. The absorption spectra are obtained using a Perkin-Elmer Lambda 950 UV/VIS/NIR spectrophotometer at 300 K. The photoluminescence spectra under UV excitations at room temperature were measured on a Perkin-Elmer LS-55 spectrofluorimeter.

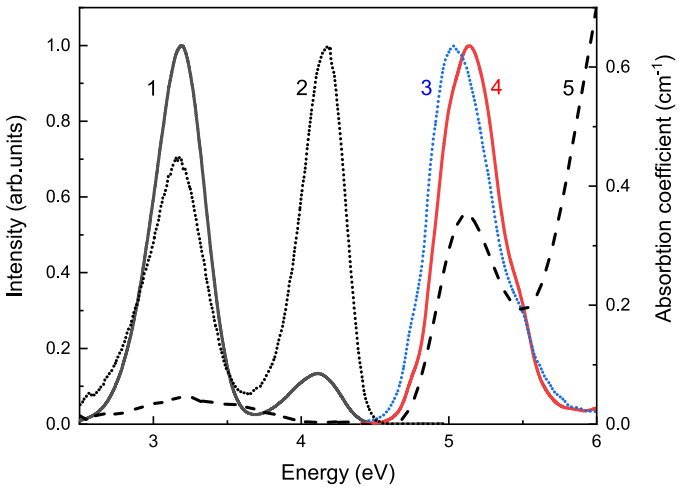

Fig. 1. Photoluminescence spectra of the sample A (curve 1) and the sample B under 5.15 eV excitation (curve 2) and excitation spectra of the sample B (curve 3) and the sample A (curve 4) monitored at 4.3 and 3.2 eV, respectively. Dashed curve 5 is the absorption spectrum. All measurements are at room temperature.

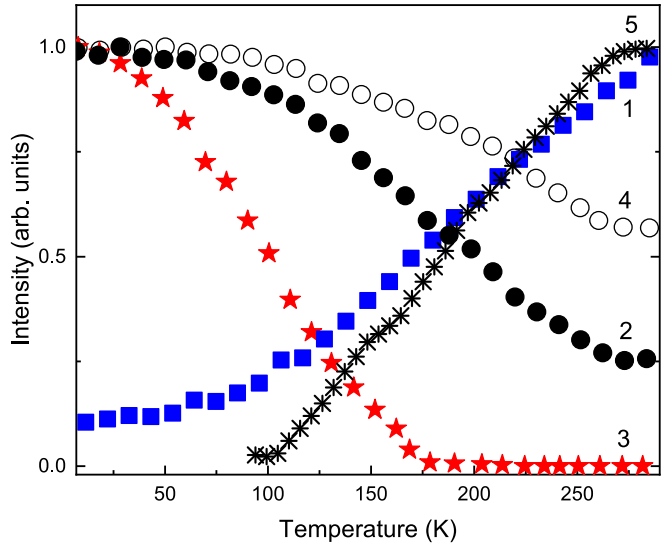

Fig. 2. Temperature dependences of luminescence bands at 3.2 eV (curve 1, blue squares), 4.3 eV (curve 2, black circles), and 2.4 eV (curve 3, red asterisks) in the sample A and temperature dependence of 4.3 eV (curve 4, empty circles) and 3.2 eV (curve 5) luminescence bands in the sample B. (For interpretation of the references to colour in this figure legend, the reader is referred to the web version of this article.)

The temperature dependences of photoluminescence spectra (10-300 K) were measured in a closed-cycle helium cryostat under a deuterium lamp Hamamtsu L7292 excitation using a VMR-2 monochromator (LOMO) with a diffraction grating of 1200 lines per mm and 4 mm slits. The luminescence was registered using a MDR2 grating monochromator with a diffraction grating of 1200 lines per mm and 2 mm slits. A photomultiplier module Hamamatsu H6780-04 was used as a photodetector.

The luminescence experiments under VUV excitations were performed using synchrotron radiation from 1.5 GeV storage ring of MAX IV synchrotron facility (Lund, Sweden). The luminescence experiments under synchrotron radiation excitations are a powerful tool for the study of wide band gap materials including glasses [27–29]. The experiments have been carried out at the photoluminescence endstation of FinEst-BeAMS beamline. The parameters of the beamline and the experimental

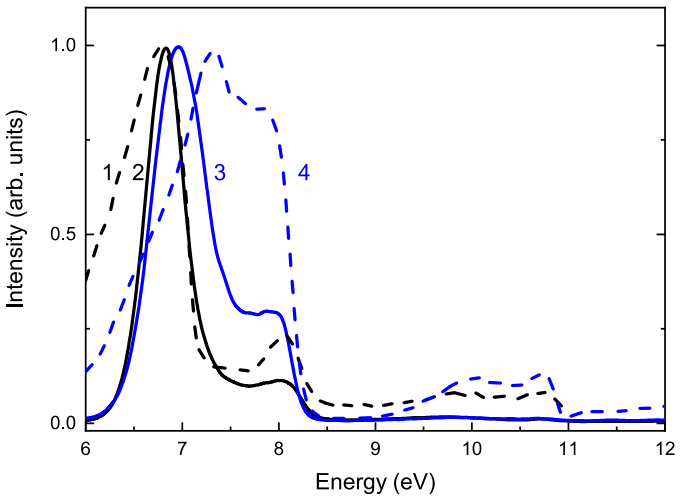

Fig. 3. Excitation spectra in VUV spectral region of the sample A monitored at 3.2 eV (curve 4) and 4.3 eV (curve 3) and the sample B monitored at 3.2 eV (curve 1) and 4.3 eV (curve 2) measured at room temperature.

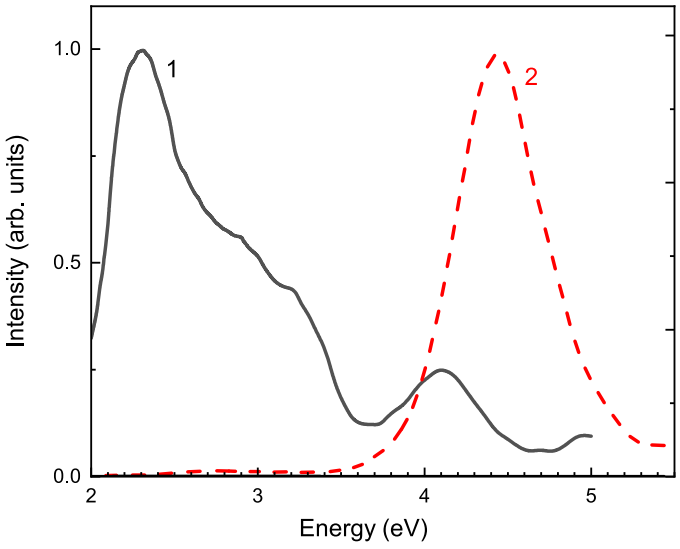

Fig. 4. Photoluminescence spectra of the sample A (curve 1) and the sample B (curve 2) under 7.5 eV excitation at 10 K.

characteristics of the endstation have been reported in details elsewhere [30–33].

The error bars in all figures are all smaller than data point symbols.

3. Experimental results

The Fig. 1 shows the luminescence and absorption spectra for the samples A and B. The photoluminescence bands peaked at 3.2 and 4.3 eV under 5.15 eV excitations are observed in the samples A and B. The optical absorption spectra of the samples exhibit the absorption band peaking at 5.1 eV and the weaker band at about 3.1 eV.

In the sample A the luminescence band at 3.2 eV is more intensive than the band at 4.3 eV. Conversely, in the sample B the intensity of the luminescence band at 4.3 eV is higher than at 3.2 eV. Furthermore, in the sample B the excitation peak of the 4.3 eV band is slightly shifted to the lower energy region and located at about 5.03 eV (Fig. 1).

After cooling down the intensity of the 3.2 eV emission band is decreased with increasing intensity of the 4.3 eV band. The temperature dependencies of the integral intensity of the 3.2 and 4.3 eV

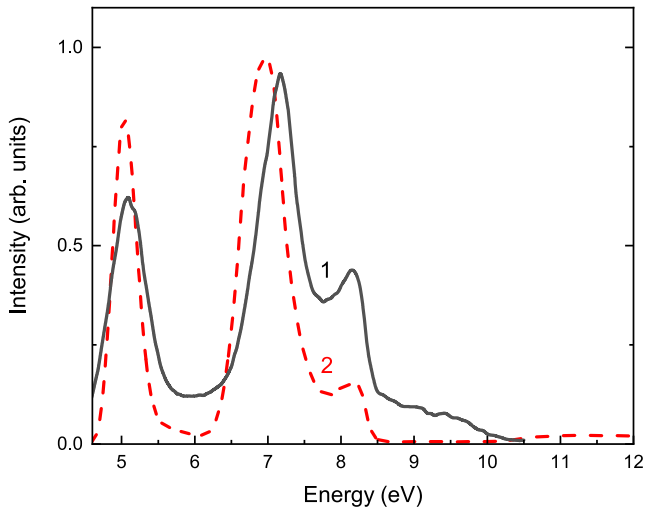

Fig. 5. Excitation spectra monitored at the 4.3 eV band of the sample A (curve 1) and the sample B (curve 2) measured at 10 K.

luminescence bands are depicted in Fig. 2 for both samples.

Excitation spectra of the samples A and B differ in the vacuum ultraviolet spectral region (VUV). Fig. 3 demonstrates the VUV excitation spectra measured at room temperature. The excitation spectrum of the sample A monitored at the 3.2 eV emission band shows a shoulder at the 6.75 eV region, an intense peak at the 7.35 eV, a dip at the 7.65 eV, and a less intensive peak at the 7.85 eV. A doublet at 10.05 and 10.70 eV was also registered. The excitation spectrum monitored at the 4.3 eV emission band of the sample A is different. The shoulder in the region of 6.75 eV disappears and the intense peak shifts towards lower energies at the 6.97 eV. The high-energy band in the region of 10 eV is not detected.

In the sample B, the excitation spectra in the high-energy region significantly differ from that one in the sample A. The excitation spectrum monitored at the 4.3 eV shows an intensive peak with a maximum at the 6.85 eV, a dip at the 7.65 eV, and a less intensive peak at the 8.05 eV. The excitation spectrum monitored at 3.2 eV is similar to the excitation spectrum for the 4.3 eV ultraviolet band. The excitation band in the region 6.85 eV is slightly shifted and peaked at the 6.75 eV. The band at the 8.05 eV and low-intensity peaks at the range of 10.05 and 10.70 eV are also found.

During cooling, the broad luminescence band peaked at 2.4 eV appears in the sample A under excitation with energies above 7.5 eV (Fig. 4). The temperature dependence of this luminescence band is shown in Fig. 2. Above 170 K this luminescence is not detected. In the sample B this luminescence is not observed.

The behavior of the 4.3 eV emission band in the samples A and B differs when the samples are cooled down. In the sample A, the maximum of this luminescence band shifts to the low-energy region, and the peak is observed at about 4.08 eV. In the sample B, the peak shifts slightly to the 4.39 eV (Fig. 4).

The excitation spectra of the 4.3 eV band measured at 10 K (Fig. 5) and at room temperature (Figs. 1 and 3) in the samples A and B are also different. In the sample A, the double excitation band was observed at 5.08 and 5.14 eV at 10 K. The next intense band peaked at the 7.17 eV at 10 K was shifted to higher energy region relative to the peak at 6.97 eV at room temperature. The dip was found at 7.8 eV and a band at 8.15 eV was also observed (Fig. 5). Thus, all excitation bands with energies above 7 eV shifted by about 0.2 eV to the high-energy region at 10 K comparing to the results at room temperature.

In the sample B, the position of the low-energy excitation band at the 5.05 eV was almost unchanged with temperature (Fig. 5). The next excitation band was peaked at the 7.0 eV. A dip is located at the 7.8 eV. In addition, the band at the 8.2 eV was found. All excitation bands with energies above 7 eV shifted by 0.15 eV to the high-energy region after

cooling down to 10 K.

4. Discussion

The observed luminescence in the samples A and B could be attributed to the luminescence of Ge-ODC(II) or GLPC [3]. On the other hand, the luminescence of the Si-ODC(II) in silica is also found in this spectral region [5]. The appearance of a significant number of ODC(II) in the studied glasses is associated with a strongly reducing atmosphere during their synthesis [34].

Assuming that the 5.0 eV absorption band is attributed to Ge-ODC (II), their concentration can be estimated according to Smakula's formula [35]. The oscillator strength is 0.097 for the S0-S1 in the Ge-ODC (II) [36]. Therefore, the concentration of Ge-ODC(II) in the samples are estimated about 1.2 ppm, which agrees with the ICP-MS data, which the Ge concentration is about 1.4 ppm. Therefore, this band can be attributed to the Ge-ODC(II).

The luminescence band peaked at the 3.2 eV corresponds to the triplet-singlet transition. The higher energy band with a maximum at the 4.3 eV is associated with the singlet-singlet transition. In the absorption and excitation spectra, the band in the 5 eV region is attributed to the singlet-singlet transition from the ground state $1A_1$ (S0) to the excited singlet state B_2 (S1). Weak absorption at 3.1 eV belongs to singlet-triplet transition. Position of 5.0 eV band in excitation spectra of the samples A and B is different at room (Fig. 1) and at 10 K (5). At low temperature non elementary structure of this band appears in the sample A (Fig. 5) but it is not observed in the sample B. Several types of ODC called α and β-ODC(II) were found in amorphous silica doped with Ge [37]. Therefore, two ODC(II) having different configurations can exist in the sample A, but only one configuration of ODC(II) is observed in the sample B.

The singlet-singlet transition corresponds to the intracenter electron transfer from a doubly occupied lone pair to a vacant π-type orbital. The higher-energy excitation bands in the 6.8-8.0 eV region are associated with the transitions to the high-energy singlet S2 states [5,6,38]. The positions of these bands are sensitive to the environment and geometry of two-fold coordinated Ge, Sn, or Si centers [39]. However, usually the energy of S0-S2 transition lies at the 7.4 eV [6,37,38]. Excitation spectra of 3.2 eV luminescence in the sample A (Figs. 3 and 5) corresponds to the literature data. Excitation band attributed to S0-S2 transition in the sample B is located at lower energy in comparison with the sample A. This is also evidence of different surrounding of ODC(II) in the samples A and B.

When the ODC(II) is excited, a non-radiative transition from the excited S1 to the triplet state occurs. This leads to the appearance of a low-energy luminescence band of 3.2 eV in silica glasses. On the other hand, an S1-S0 transition attributed to the luminescence band at the 4.3 eV takes place. In the model of the electronic structure of ODC(II) proposed in [34] where the transition of an electron from the excited singlet S1 state to the triplet T1 state is accompanied by the barrier which can be estimated from the temperature dependence of the 3.2 eV band (Fig. 2). Arrhenius energy of barrier is about 170 meV, which agrees with the data on ODC(II) in silica glasses [9,40]. The origin of excited states of the ODC(II) in non-crystalline solids has been still discussed, but it is noted that they are largely similar to those observed in structurally similar crystalline matrices [1].

At room temperature, the sample A exhibits mainly the triplet-singlet luminescence due to thermally activated intersystem crossing. This process becomes less effective when a sample is cooled down. The intensity of the triplet-singlet luminescence decreases, while the intensity of the S1-S0 luminescence increases. In the sample B, the ratio of luminescence band intensities associated with the triplet-singlet and singlet-singlet luminescence differs from the sample A. It is unusual for silica glasses. In the sample B, the luminescence associated with S1-S0 transitions is the most intense already at room temperature, whereas the intensity of the triplet band at the 3.2 eV is much lower. Nevertheless, during the cooling process, its temperature dependency is similar to that of the same band in the sample A. Previously, similar effects were observed in irradiated glasses [14,41] and various combinations of thermal treatment of glasses and their irradiation [42] or annealing of samples in hydrogen atmosphere [2]. The observed effects were ascribed to a violation of the stoichiometry of the glasses during irradiation, evaporation of germanium from the glass surface, and sample inhomogeneity. However, samples studied in this article have the same synthesis procedure and concentration of ODC(II), as we estimated from the absorption spectra. Therefore, the differences in the luminescence spectra cannot be explained by stoichiometry and inhomogeneity causes.

On the other hand, the excitation spectra of the triplet and singlet luminescence in the sample A are different in the region of 6–11 eV. As it was pointed in [43], the high-energy excited states of the Ge-ODC(II) has the excitonic origin. We suggest that two types of differently oriented Ge-ODC(II) exist. Their excitation spectra differ in the region of 6–10 eV and the thermally stimulated cross-relaxation efficiency from S2 to triplet state is significantly higher for one configuration than for another one when S0-S2 is excited.

The excitation spectra of the singlet and triplet luminescence in the sample B at room temperature are identical. This may indicate that only one configuration of the ODC(II) is found in the sample B, as well as in the more symmetric polymorphic modifications of quartz: cristobalite [43]. Thus, we can assume that the local environment of the ODC(II) in the samples A and B are different. In the sample B, the ODC(II) has higher symmetry, which leads to the formation of only one type of ODC (II), whereas in the sample A, the ODC(II) symmetry is lower and close to α-quartz, so two types of ODC(II) are observed. This assumption is also supported by the fact that the excitation spectra of the samples A and B differ in the low-energy band. In contrast to the sample A the excitation band at 5.0 eV observed in the sample B has lower energy tail.

When cooled down to a temperature of 10 K, the triplet luminescence in the studied glasses disappears. At the same time, in the sample A an intense luminescence in the 2.4 eV region appears upon excitation at 10 eV, which is related to the luminescence of self-trapped excitons in the silica [43,44]. Early, the threshold of self-trapped exciton luminescence was estimated at the 8.3 eV in high purity silica glasses. In the sample A self-trapped exciton luminescence was excited at lower energy due to presence of Ge impurity. In this case, self-trapped excitons could be perturbed by Ge impurities.

Self-trapped exciton luminescence is not registered in the sample B. Previously, this has been observed in cristobalite ceramics [45]. Moreover, the singlet luminescence is shifted to higher energies in crystalline cristobalite glass. The high-energy excitation bands of the ODC(II) in quartz and cristobalite in the region of 7 eV differ, which is caused by the difference in the surrounding geometry and, accordingly, in the configuration of the impurity trapped exciton in quartz and cristobalite [43]. The presence of the band in 8 eV region in all samples is the evidence that higher energy excited states of ODC(II) has an excitonic origin.

A dip at the 7.8 eV observed in all samples is due to appearance of strong absorption band peaked at 7.6 eV in an amorphous silica. This optical absorption band is assigned to $\sigma - \sigma^*$ transition of the Si-Si bond [46]. This absorption appears in the samples due to synthesis in highly reducing atmosphere that results in the formation of Si-Si bonds.

Higher energy bands in excitation spectra measured at room temperature in the region 9.5–11 eV is attributed to delocalized excitonic states retained their delocalized properties albeit thermal and structural disorder which is typical of an amorphous material [47].

Under excitation below 7.8 eV intracenter transitions modified by inhomogeneous broadening of non-equivalent centers occur in silica glasses. These electronic excitations are localized and short-range order plays important role in the excitation band positions in the excitation spectra. For higher energy excitation (>7.8 eV) inter center excitation dominates. These electronic excitations is highly delocalized. Therefore, the corresponding bands in excitation spectra have the same positions in

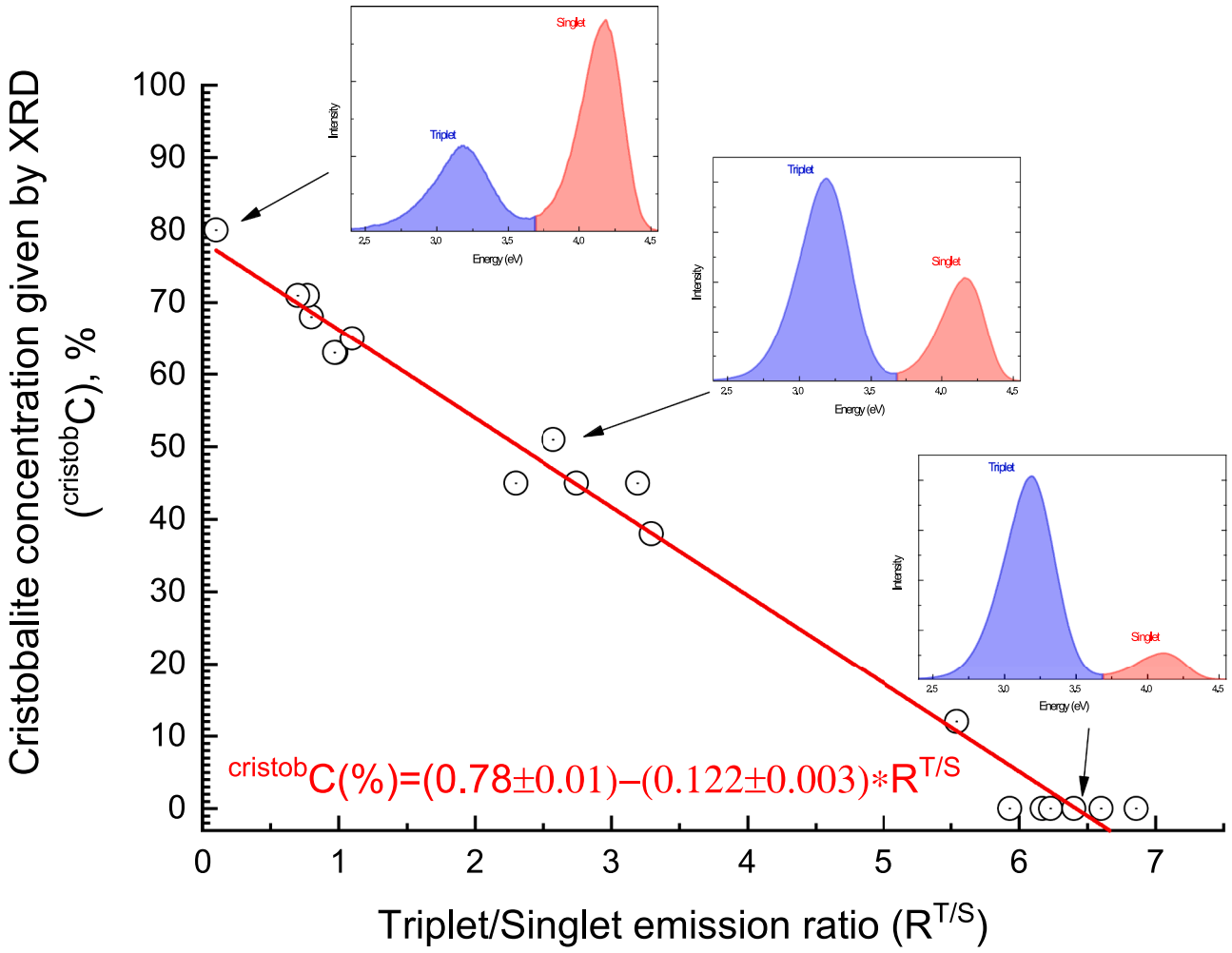

Fig. 6. Correlation between the ratio of singlet-triplet emission bands and cristobalite concentration (in wt%) in the raw material.

both type of glasses.

In silica glasses synthesized from the raw materials containing a quartz and cristobalite, the ratio of the triplet and singlet luminescence peaks correlated with the content of cristobalite in the raw materials. As the proportion of cristobalite in the raw material increased, the intensity of singlet luminescence is increased too, while the intensity of the triplet luminescence degrades. The linear dependence between phase composition in the raw materials and the singlet/triplet luminescence intensity relationship could be constructed and shown in 6. The highest concentration of cristobalite corresponds to the sample B. The sample A contains 0% cristobalite.

As a result, we can conclude that the observed differences in the luminescence and excitation spectra of ODC(II) in the samples A and B indicate that the environment of ODC(II) and, therefore, short-range order in the samples A and B are different. In a sense, the glass inherits the structure of the raw material. In the case of the sample B, that was manufactured mainly of cristobalite, the short-range order is more symmetrical in comparison with the sample A prepared from an α-quartz. A similar effect was observed in irradiated glasses where the different configuration of E' centers were determined by the ESR in cristobalite and quartz glasses [21].

5. Conclusion

The study of ODC(II) luminescence in cristobalite and quartz glasses prepared from a natural raw material was carried out. It was found that the relationship between singlet and triplet luminescence bands of ODC (II) in these glasses significantly differs. The intensity of the singlet band increases with an increase of the cristobalite content in the raw material.

Based on the study of the excitation spectra of the glasses, we found that the observed changes in the ratio of the singlet and triplet luminescence are associated with a difference in the short-range order.

CRediT authorship contribution statement

Tatiana Garmysheva: Writing – original draft, Conceptualization, Methodology, Investigation. **Alexander I. Nepomnyashchikh:** Supervision, Funding acquisition, Resources, Writing – review & editing, Conceptualization. **Alexey Shalaev:** Writing – review & editing, Conceptualization. **Ekaterina Kaneva:** Writing – original draft, Investigation, Methodology. **Alexey Paklin:** Resources. **Kirill Chernenko:** Writing – review & editing, Methodology, Investigation. **Anna P. Kozlova:** Investigation, Writing – review & editing, Funding acquisition. **Vladimir Pankratov:** Conceptualization, Methodology, Investigation, Writing – review & editing. **Roman Shendrik:** Conceptualization, Methodology, Writing – original draft, Writing – review & editing, Investigation, Formal analysis, Validation, Visualization.

Declaration of Competing Interest

The authors declare that they have no known competing financial interests or personal relationships that could have appeared to influence the work reported in this paper.

Acknowledgments

This study was performed under the project 0284-2021-0004 "Materials and Technologies for the Development of Radiation Detectors, Luminophores, and Optical Glasses". The authors wish to thank the Isotope-geochemical research center for Collective Use (A. P. Vinogradov Institute of Geochemistry of the Siberian Branch of the Russian Academy of Sciences).

The research leading to this result has been supported by the project CALIPSO plus under the Grant Agreement 730872 from the EU Framework Programme for Research and Innovation HORIZON 2020.

The Institute of Solid State Physics, University of Latvia as the Center of Excellence has received funding from the H2020-WIDESPREAD-01-2016-2017-TeamingPhase2 under grant agreement No. 739508, project CAMART2.

Supplementary material

Supplementary material associated with this article can be found, in the online version, at doi:10.1016/j.jnoncrysol.2021.121199.

References

[1] A.N. Trukhin, Localized states in wide-gap glasses. comparison with relevant crystals, J Non Cryst Solids 189 (1–2) (1995) 1–15, https://doi.org/10.1016/0022-3093(95)00207-3.
[2] A.N. Trukhin, Luminescence of localized states in silicon dioxide glass. a short review, J Non Cryst Solids 357 (8–9) (2011) 1931–1940, https://doi.org/10.1016/j.jnoncrysol. 2010.10.041.
[3] L. Skuja, M. Hirano, H. Hosono, K. Kajihara, Defects in oxide glasses, physica status solidi (c) 2 (1) (2005) 15–24, https://doi.org/10.1002/pssc.200460102.
[4] M. D'Amico, F. Messina, M. Cannas, M. Leone, R. Boscaino, Photoluminescence spectral dispersion as a probe of structural inhomogeneity in silica, J. Phys.: Condens. Matter 21 (11) (2009) 115803, https://doi.org/10.1088/0953-8984/21/11/115803.
[5] L.N. Skuja, A.N. Streletsky, A.B. Pakovich, A new intrinsic defect in amorphous SiO_2: twofold coordinated silicon, Solid State Commun 50 (12) (1984) 1069–1072, https://doi.org/10.1016/0038-1098(84)90290-4.
[6] L. Skuja, Direct singlet-to-triplet optical absorption and luminescence excitation band of the twofold-coordinated silicon center in oxygen-deficient glassy SiO_2, J Non Cryst Solids 167 (3) (1994) 229–238, https://doi.org/10.1016/0022-3093(94)90245-3.
[7] A.N. Trukhin, A. Sharakovski, J. Grube, D.L. Griscom, Sub-band-gap-excited luminescence of localized states in SiO_2 – Si and SiO_2 – Al glasses, J Non Cryst Solids 356 (20–22) (2010) 982–986, https://doi.org/10.1016/j.jnoncrysol.2010.01.027.
[8] A.N. Trukhin, K.M. Golant, Y. Maksimov, M. Kink, R. Kink, Recombination luminescence of oxygen-deficient centers in silica, J Non Cryst Solids 354 (2–9) (2008) 244–248, https://doi.org/10.1016/j.jnoncrysol.2007.07.060.
[9] Y. Nagayoshi, R. Matsuzaki, T. Uchino, Multiple intersystem crossing processes in Ge-doped silica glass: emission mechanism of 2-fold coordinated Ge atoms, The Journal of Physical Chemistry C 122 (41) (2018) 23712–23719, https://doi.org/10.1021/acs.jpcc.8b08162.
[10] T. Uchino, M. Takahashi, T. Yoko, Structure and formation mechanism of Ge-E' center from divalent defects in Ge-doped SiO_2 glass, Phys. Rev. Lett. 84 (7) (2000) 1475, https://doi.org/10.1103/physrevlett.84.1475.
[11] X. Guan, R. Zhang, B. Jia, X. Chen, B. Yan, G.-D. Peng, S. Li, P. Lu, Electronic and optical properties of Ge-doped silica optical fiber, Mod. Phys. Lett. B 33 (12) (2019) 1950150, https://doi.org/10.1142/s0217984919501501.
[12] M. D'Amico, F. Messina, M. Cannas, M. Leone, R. Boscaino, Isoelectronic series of oxygen deficient centers in silica: experimental estimation of homogeneous and inhomogeneous spectral widths, The Journal of Physical Chemistry A 112 (47) (2008) 12104–12108, https://doi.org/10.1021/jp805372u.
[13] A. Cannizzo, S. Agnello, R. Boscaino, M. Cannas, F.M. Gelardi, S. Grandi, M. Leone, Role of vitreous matrix on the optical activity of Ge-doped silica, J. Phys. Chem. Solids 64 (12) (2003) 2437–2443, https://doi.org/10.1016/s0022-3697(03)00287-7.
[14] H.-J. Fitting, T. Barfels, A.N. Trukhin, B. Schmidt, A. Gulans, A. Von Czarnowski, Cathodoluminescence of Ge^+, Si^+, and O^+ implanted SiO_2 layers and the role of mobile oxygen in defect transformations, J Non Cryst Solids 303 (2) (2002) 218–231, https://doi.org/10.1016/s0022-3093(02)00952-3.
[15] S. Agnello, R. Boscaino, M. Cannas, F.M. Gelardi, M. Leone, UV And vacuum-UV properties of ge related centers in gamma irradiated silica, Radiat. Eff. Defects Solids 157 (6–12) (2002) 615–619, https://doi.org/10.1080/10420150215808.
[16] Z.W. Wu, M.Z. Li, W.H. Wang, K.X. Liu, Hidden topological order and its correlation with glass-forming ability in metallic glasses, Nat Commun 6 (1) (2015) 1–7, https://doi.org/10.1038/ncomms7035.
[17] A.N. Trukhin, Luminescence of SiO_2 and GeO_2 crystals with rutile structure. comparison with α-quartz crystals and relevant glasses, Low Temp. Phys. 42 (7) (2016) 561–569, https://doi.org/10.1063/1.4959014.
[18] A. Trukhin, B. Poumellec, J. Garapon, Luminescence decay kinetics of Ge related center in silica, Radiat. Eff. Defects Solids 149 (1–4) (1999) 89–95, https://doi.org/10.1080/10420159908230138.
[19] S. Agnello, R. Boscaino, M. Cannas, A. Cannizzo, F.M. Gelardi, S. Grandi, M. Leone, Spectral heterogeneity of oxygen-deficient centers in ge-doped silica, Radiat Meas 38 (4–6) (2004) 645–648, https://doi.org/10.1016/j.radmeas.2003.12.014.
[20] A.I. Nepomnyashchikh, A.A. Shalaev, T.Y. Sizova, A.S. Paklin, A.N. Sapozhnikov, L. A. Pavlova, Onset temperatures and kinetics of quartz glass crystallization, Crystallogr. Rep. 63 (2) (2018) 290–294, https://doi.org/10.1134/S1063774518020153.
[21] R.I. Mashkovtsev, A.I. Nepomnyashchikh, A.P. Zhaboedov, A.S. Paklin, Epr study of the E'-defects in optical glasses and cristobalite, EPL (Europhysics Letters) 133 (1) (2021) 14003, https://doi.org/10.1209/0295-5075/133/14003.
[22] E.I. Vorob'ev, A.M. Spiridonov, A.I. Nepomnyashchikh, M.I. Kuz'min, Superpure quartzites of the Eastern Sayan (Burayt Republic, Russia), Dokl. Earth Sci. 390 (4) (2003) 497–500.
[23] A.M. Fedorov, V.A. Makrygina, A.I. Nepomnyaschikh, A.P. Zhaboedov, A. V. Parshin, V.F. Posokhov, Y.V. Sokolnikova, Geochemistry and petrology of superpure quartzites from East Sayan Mountains, Russia, Acta Geochimica (2018) 1–18, https://doi.org/10.1007/s11631-018-0268-5.
[24] A.I. Nepomnyashchikh, T.V. Demina, A.P. Zhaboedov, I.A. Eliseev, P.A. Lesnikov, A.K. Lesnikov, A.S. Paklin, V.S. Romanov, A.N. Sapozhnikov, Y.V. Sokol'nikova, et al., Optical silica glass based on super quartzites from the eastern sayan mountains, Glass Phys. Chem 43 (3) (2017) 222–226, https://doi.org/10.1134/S1087659617030099.
[25] R.A. Young, The rietveld method (IUCr monograph on crystallography), Oxford University Press, 1993.
[26] Bruker AXS TOPAS V4: General profile and structure analysis software for powder diffraction data: User manual, Bruker AXS, 2008.
[27] V. Pankratova, A.P. Kozlova, O.A. Buzanov, K. Chernenko, R. Shendrik, A. Šarakovskis, V. Pankratov, Time-resolved luminescence and excitation spectroscopy of co-doped $Gd_3Ga_3Al_2O_12$ scintillating crystals, Sci Rep 10 (1) (2020) 1–11, https://doi.org/10.1038/s41598-020-77451-x.
[28] A. Tuomela, M. Zhang, M. Huttula, S. Sakirzanovas, A. Kareiva, A.I. Popov, A. P. Kozlova, S.A. Aravindh, W. Cao, V. Pankratov, Luminescence and vacuum ultraviolet excitation spectroscopy of samarium doped SrB_4O_7, J Alloys Compd 826 (2020) 154205, https://doi.org/10.1016/j.jallcom.2020.154205.
[29] A. Shalaev, R. Shendrik, A. Rusakov, A. Bogdanov, V. Pankratov, K. Chernenko, A. Myasnikova, Luminescence of divalent lanthanide doped BaBrIsingle crystal under synchrotron radiation excitations, Nucl. Instrum. Methods Phys. Res., Sect. B 467 (2020) 17–20, https://doi.org/10.1016/j.nimb.2020.01.023.
[30] K. Chernenko, A. Kivimäki, R. Pärna, W. Wang, R. Sankari, M. Leandersson, H. Tarawneh, V. Pankratov, M. Kook, E. Kukk, et al., Performance and characterization of the finestbeams beamline at the MAX IV laboratory, J Synchrotron Radiat 28 (5) (2021), https://doi.org/10.1107/S1600577521006032.
[31] R. Pärna, R. Sankari, E. Kukk, E. Nõmmiste, M. Valden, M. Lastusaari, K. Kooser, K. Kokko, M. Hirsimäki, S. Urpelainen, et al., Finestbeams–a wide-range finnish-estonian beamline for materials science at the 1.5 GeV storage ring at the MAX IV laboratory, Nucl. Instrum. Methods Phys. Res., Sect. A 859 (2017) 83–89, https://doi.org/10.1016/j.nima.2017.04.002.
[32] V. Pankratov, A. Kotlov, Luminescence spectroscopy under synchrotron radiation: from SUPERLUMI to FINESTLUMI, Nucl. Instrum. Methods Phys. Res., Sect. B 474 (2020) 35–40, https://doi.org/10.1016/j.nimb.2020.04.015.
[33] V. Pankratov, R. Pärna, M. Kirm, V. Nagirnyi, E. Nõmmiste, S. Omelkov, S. Vielhauer, K. Chernenko, L. Reisberg, P. Turunen, A. Kivimäki, E. Kukk, M. Valden, M. Huttula, Progress in development of a new luminescence setup at the finestbeams beamline of the MAX IV laboratory, Radiat Meas 121 (2019) 91–98, https://doi.org/10.1016/j.radmeas.2018.12.011.
[34] A.V. Amossov, A.O. Rybaltovsky, Oxygen-deficient centers in silica glasses: a review of their properties and structure, J Non Cryst Solids 179 (1994) 75–83, https://doi.org/10.1016/0022-3093(94)90686-6.
[35] A. Smakula, Über erregung und entfärbung lichtelektrisch leitender alkalihalogenide, Zeitschrift für Physik 59 (9) (1930) 603–614, https://doi.org/10.1007/BF01344801.
[36] D.L. Griscom, On the natures of radiation-induced point defects in GeO_2 – SiO_2 glasses: reevaluation of a 26-year-old ESR and optical data set, Opt Mater Express 1 (3) (2011) 400–412, https://doi.org/10.1364/OME.1.000400.
[37] A.F. Zatsepin, H.-J. Fitting, V.S. Kortov, V.A. Pustovarov, B. Schmidt, E.A. Buntov, Photosensitive defects in silica layers implanted with germanium ions, J Non Cryst Solids 355 (1) (2009) 61–67, https://doi.org/10.1016/j.jnoncrysol.2008.08.025.
[38] L. Skuja, Isoelectronic series of twofold coordinated Si, Ge, and Sn atoms in glassy SiO_2: a luminescence study, J Non Cryst Solids 149 (1–2) (1992) 77–95, https://doi.org/10.1016/0022-3093(92)90056-P.
[39] G. Pacchioni, L. Skuja, D.L. Griscom, Defects in SiO_2 and related dielectrics: Science and technology volume 2, Springer Science & Business Media, 2012.
[40] A. Trukhin, B. Poumellec, Energy transport in silica to oxygen-deficient luminescence centers. comparison with other luminescence centers in silica and α-quartz, Solid State Commun 129 (5) (2004) 285–289, https://doi.org/10.1016/j.ssc.2003.10.027.
[41] A.N. Trukhin, A. Boukenter, Y. Ouerdane, S. Girard, γ-ray induced GeODC(II) centers in germanium doped α-quartz crystal, J Non Cryst Solids 357 (16–17) (2011) 3288–3291, https://doi.org/10.1016/j.jnoncrysol.2011.04.011.

[42] A. Alessi, S. Agnello, F.M. Gelardi, A. Parlato, S. Grandi, Concentration growth and thermal stability of γ-ray induced germanium lone pair center in Ge-doped sol-gel $\alpha - SiO_2$, J Non Cryst Solids 355 (2009) 1050–1053, https://doi.org/10.1016/j.jnoncrysol.2008.11.032.
[43] A.N. Trukhin, Excitons in SiO_2: a review, J Non Cryst Solids 149 (1–2) (1992) 32–45, https://doi.org/10.1016/0022-3093(92)90052-l.
[44] C. Itoh, K. Tanimura, N. Itoh, Optical studies of self-trapped excitons in SiO_2, J. Phys. C: Solid State Phys. 21 (26) (1988) 4693, https://doi.org/10.1088/0022-3719/21/26/017.
[45] A.N. Trukhin, K. Smits, J. Jansons, A. Kuzmin, Luminescence of polymorphous SiO_2, Radiat Meas 90 (2016) 6–13, https://doi.org/10.1016/j.radmeas.2015.12.002.
[46] H. Hosono, Y. Abe, H. Imagawa, H. Imai, K. Arai, Experimental evidence for the Si-Si bond model of the 7.6-eV band in SiO_2 glass, Physical Review B 44 (21) (1991) 12043, https://doi.org/10.1103/PhysRevB.44.12043.
[47] F. Messina, E. Vella, M. Cannas, R. Boscaino, Evidence of delocalized excitons in amorphous solids, Phys. Rev. Lett. 105 (11) (2010) 116401, https://doi.org/10.1103/PhysRevLett.105.116401.